Coupling Effect of Multicavity on Flame Stabilization Mode Transitions in Scramjet Combustor

Zhenjie Wu,* Qifan Zhang,[†] and Fangyou Yu[‡]
*State Key Laboratory of High Temperature Gas Dynamics, Chinese Academy of Sciences,
100190 Beijing, People's Republic of China*
Weihang Luo[§]
Chinese Academy of Sciences, 100190 Beijing, People's Republic of China
and
Zhanbiao Gao[¶] and Lianjie Yue[**]
*State Key Laboratory of High Temperature Gas Dynamics, Chinese Academy of Sciences,
100190 Beijing, People's Republic of China*

To investigate the effect of the multicavity on flame stabilization mode transition in a scramjet combustor, experiments involving various fuel injection strategies were conducted in a direct-connect supersonic combustor with a multicavity at the entrance with a Mach number of 3.0. The flame stabilization mode of the first cavity transitioned under all working conditions, but the equivalence ratio and wall static pressure changes were different. According to the different driving modes, the transition types were identified to be direct-driven local heat release and indirect-driven downstream backpressure. Direct changes in the local equivalence ratio could lead to significant combustion variations. The difference in combustion intensity between the two flame stabilization modes resulted in obvious path dependence, and the different transition paths of the flame stabilization mode could yield a difference in the equivalence ratio of $\Delta\Phi = 0.10$ at the moment of flame stabilization mode transition. If the equivalence ratio of the first cavity was set to a low value, the backpressure generated by downstream combustion was indirectly employed to promote the flame stabilization mode transition of the first cavity, which could reduce the degree of abrupt change. In addition, different transition paths could generate a difference in the equivalence ratio of $\Delta\Phi = 0.03$ at the moment of flame stabilization mode transition.

Nomenclature

Φ	=	equivalence ratio
Ma	=	Mach number
p	=	static pressure, kPa

Subscripts

C	=	cavity shear-layer stabilized combustion
J	=	jet-wake stabilized combustion
t	=	total
1	=	the first cavity
2	=	the second cavity

Superscripts

a	=	abrupt change
f	=	final
i	=	initial

*Ph.D. Candidate, Institute of Mechanics; also School of Engineering Sciences, University of the Chinese Academy of Sciences, Chinese Academy of Sciences, 100049 Beijing, People's Republic of China.
†Research Assistant, Institute of Mechanics; zhangqifan@imech.ac.cn (Corresponding Author).
‡M.E. Student, Institute of Mechanics; also School of Engineering Sciences, University of the Chinese Academy of Sciences, Chinese Academy of Sciences, 100049 Beijing, People's Republic of China.
§Junior Engineer, Institute of Mechanics.
¶Engineer, Institute of Mechanics.
**Professor, Institute of Mechanics; also School of Engineering Sciences, University of the Chinese Academy of Sciences, Chinese Academy of Sciences, 100049 Beijing, People's Republic of China.

I. Introduction

AS AN ideal propulsion system for airbreathing hypersonic vehicles, scramjet engines have been drawing increasing attention. Flame stabilization in the scramjet engine is one of the most basic and key problems of supersonic combustions, owing to the short residence time of supersonic airflow. Various flame stabilization strategies are thereby used and implemented in scramjets, such as structs [1,2], ramps [3], and cavities [4–7] in which the cavities are widely applied in combustor design for their advantages of a high mixing efficiency, long fuel residence time, low drag, and simple structure [8–11].

The flame stabilization mode of combustors influenced by a single cavity has been extensively studied. Micka and Driscoll [12,13] found that different total temperatures of the incoming flow induce two different flame stabilization modes, namely, the cavity stabilized combustion at a low total temperature because the flame was stabilized in the shear layer of the cavity, and the jet wake stabilized combustion at a high total temperature with the flame stabilized within a short distance downstream of the fuel injection point. Sun et al. [14] explained the mechanism of the flame stabilization mode through both experiments and simulations. The characteristics of the pressure distributions under different flame stabilization modes were quite different in the experimental study of Yuan et al. [15]. Zhang et al. [16,17] experimentally and numerically observed abrupt changes in the wall pressure and thrust during the transition process of the flame stabilization modes in the combustor with a pair of cavities. In addition, the nonlinear mode transition showed apparent path dependence, which indicated that the characteristics of the current state were affected by the historical evolution path. Path dependence of the flame stabilization mode transition and abrupt change characteristics caused the flowfield evolution process to become rather complex, whereas the induced dual solution of the flame stabilization mode is undesirable in actual engine control systems.

The multicavity structure exhibits higher engineering research values for its combustion efficiency and wide-speed range adaptability than the single cavity. The concerning phenomena of a

combustor with a multicavity or a single cavity are fundamentally different, such as the fuel mixing [18], the ignition process [19], the flame structure [20,21], and the flame stabilization mechanism [22]. Situ et al. [23] performed a large number of experiments to evaluate flameholding and mixing enhancement of kerosene-fueled supersonic reactive flow in a combustor with a tandem dual cavity. Numerous studies [24–27] demonstrated that the application of a multicavity instead of a single cavity in flame stabilization could improve the efficient combustion and engine performance because the unburned fuel in the first cavity tends to burn in the second cavity, and thereby promotes fuel mixing and flame stability [28].

The coupling effect of multicavity in a combustor is very important. However, few studies focused on the transition process of the flame stabilization mode of the combustor influenced by a multicavity. Furthermore, how the path dependence characteristics associated with the flame stabilization mode transition observed in combustors with a single cavity evolve for the counterpart with a multicavity is of interest and a question to be answered. In this paper, the flame stabilization mode transition process and the pressure change characteristics of combustors with multicavities were examined via well-designed fuel injection strategies.
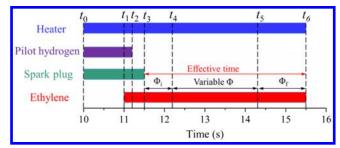
II. Experimental Approach

A. Direct-Connect Supersonic Combustion Facility and Combustor Model

The experiments were conducted at the direct-connect supersonic combustion facility. This facility can simulate the inlet flow conditions of combustors by burning hydrogen under oxygen replenishment conditions. High-pressure air, oxygen, and hydrogen are quantitatively controlled through a pressure-reducing valve and flowmeter in sequence, and then they enter a heater for the combustion to provide the required pressure and temperature conditions with a specific mole percentage of oxygen of 21%. Upstream of the test section, a Laval nozzle is installed to accelerate the high-enthalpy flow to a certain Mach number. To ensure the safety of the experiment, gas flowing from the test section enters the exhaust pipe section and is discharged into the outside environment. The combustor inlet parameters are shown in Table 1. The test Mach number is 3.0, and the total temperature and total pressure are 1657 K and 2.10 MPa, respectively. This test condition of the direct-connect supersonic combustor corresponds to the flight condition of Mach 6 at an altitude of 27 km. The inflow static pressure is 42.0 kPa, which is also used as a reference pressure for the normalization of the wall pressure.

The timing control scheme of the experiment is shown in Fig. 1. The effective running time of the heater in the test was $t_0 - t_6$, which lasted 5.5 s. To ensure the successful ignition, flammable hydrogen
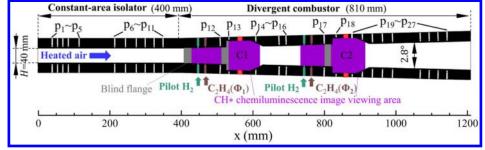
with a high calorific value was injected into the section to ignite the subsequently injected ethylene. Hydrogen injection was initiated at $t_o = 10.0$ s, and the spark plug was activated simultaneously. Then, the hydrogen injection and spark plug operation were terminated at $t_2 = 11.2$ s and $t_3 = 11.5$ s, respectively. Moreover, ethylene injection was started at $t_1 = 11.0$ s and stopped at $t_6 = 15.5$ s. As observed, the injection of ethylene was only sustained for a total of 4.0 s from t_3 to t_6, and this stage represents the effective time of ethylene combustion. The test adopted a stepwise equivalence ratio continuous change step; namely, the initial equivalence ratio Φ^i was maintained from $t_3 = 11.5$ s to $t_4 = 12.2$ s, the continuous change stage of the equivalence ratio ranged from $t_4 = 12.2$ s to $t_5 = 14.3$ s, and the final equivalence ratio Φ^f was sustained from t_5 to t_6, respectively.
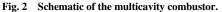
To explore the coupling effect between multicavities, the two-dimensional symmetrical combustor model adopts the design of a rectangular combustor with two pairs of cavities: C1 and C2, as shown in Fig. 2. The combustor model is 80 mm in width, and it only expands up and down symmetrically. The length, height, and width of the isolator are 400, 40, and 80 mm, respectively, in which the isolator has a constant sectional area and is connected by an 810-mm-long divergent test section with a double-sided expansion angle of 2.8 deg. The first cavity (C1) and second cavity (C2) are mounted in the divergent test section, and the structs of the cavities are completely the same, as shown in Fig. 3. The depth and the bottom length of each cavity are 17 and 65 mm, respectively. The length-to-depth ratio of the cavity is about 3.8, and it is termed "open" [29], which is also the most commonly used cavity type in scramjets. In addition, the bottom side of each cavity is equipped with a spark plug, and the spark plug of each cavity can be controlled independently. Upstream of each cavity, there exist two rows of fuel injection orifices, which are ethylene and hydrogen orifices that are, respectively, located at distances of 60 and 80 mm to the cavity fore wall. Five 1.2-mm-diameter orifices are used for ethylene injection and four 1.0-mm-diameter orifices are used for hydrogen injection, which is implemented along the spanwise direction with an interval of 15 mm.

B. Measurement Techniques

As shown in Fig. 2, to measure the wall pressure in the combustor, 27 pressure measuring holes with diameters of 0.8 mm and depths of 3.0 mm are implemented on both the upper and lower walls. These measuring points are located along the centerline of the model by using the traditional wall static pressure measurement method, which is equipped with an ESP-32HD electronic pressure scanning valve and a DTC Initium pressure acquisition system (PSI Company) with an accuracy of 0.25% full scale and a sampling frequency of 652 Hz. In addition, the widely used noncontact CH* self-luminescence measurement method [30] measuring the heat release rate of combustion is applied in the flame measurement [31–33]. In the experiment, a filter with a wavelength of 430 ± 15 nm and a peak transmittance of 0.882 is added to the high-speed camera to capture light at a wavelength of 431 nm, namely, the luminous intensity of CH*. The shooting area covers the multicavity and upstream areas, as shown in Fig. 2. The high-speed camera is a v1612 camera from the Phantom Company, which is operated at 4000 frames per second with a resolution of 1280×800 pixels and a shutter time of 50 μs.

The dynamic adjustment of the mass flow of ethylene adopts an electric pressure regulating valve, and the ethylene flow rate is thereby determined through a differential pressure orifice flowmeter. The range of the differential pressure transmitter is $0.4 \sim 40$ kPa, and the accuracy is about 0.1% full scale to ensure the accurate flow measurement. Ethylene at the first and second positions is independently controlled and measured through different electric pressure regulating valves and flow measurement systems. Furthermore, the same transistor–transistor logic signal is applied to trigger all measurement systems to ensure triggering synchronization, and the acquisition time of each measurement system covers the entire validity period of the experiment.
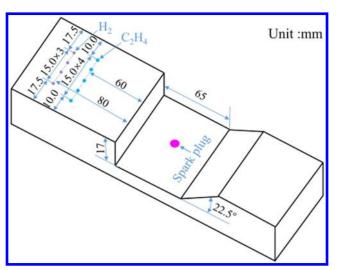
Table 1   Test conditions

Parameter	Value
Ma	3.0
Total temperature, K	1657
Total pressure, MPa	2.10

Fig. 1   Brief description of the experimental steps and the time sequence.

Fig. 2 Schematic of the multicavity combustor.

Fig. 3 Schematic of the cavity.

C. Fuel Injection Schemes

To study the effects of the multicavity on the process of flame stabilization mode transition, three equivalence ratio adjustment strategies were designed: each of which includes two comparative experiments with opposite changing rules of the equivalence ratio. The equivalence ratio adjustment parameters for each test are summarized in Table 2, in which Φ_1, Φ_2, and Φ_t denote the ethylene equivalence ratio injected upstream of the first cavity, the equivalence ratio injected upstream of the second cavity, and the total equivalence ratio, respectively. In the first group corresponding to tests A1 and A2, it serves as a reference case that ethylene is only injected upstream of the first cavity with varying equivalence ratios and no injection for the second cavity. In the second group corresponding to tests A3 and A4, the equivalence ratio of the first cavity varies, whereas it remains a constant for the second cavity. To study the effect of combustion in the second cavity on the flame stabilization mode transition of the first cavity, in the third group corresponding to tests A5 and A6, the equivalence ratio of the second cavity is varied, whereas a constant equivalence ratio is maintained upstream of the first cavity to evaluate that how the downstream burning zone driving flame stabilization mode transition in the upstream burning zone. Because the penetration depth of ethylene fuel has not been measured in the experiment, we can calculate penetration depth of the first injection point through the empirical formula obtained from the article of Ref. [34]. The penetration depth of the highest equivalence

ratio is 13.1 mm at the leading edge of the first cavity, and the penetration depth accounts for 56.6% of the half-height of the local section. The penetration depth when the equivalence ratio is 0.05 also reaches 5.1 mm, ensuring a certain penetration depth at the lowest equivalence ratio.

III. Results and Discussion

A. Ethylene Injection Upstream of the First Cavity

To facilitate comparison to the subsequent tests, the pressure and flame variation characteristics of the combustor were studied by injecting fuel only upstream of the first cavity. The equivalence ratio is set to increase in test A1 and decrease in test A2. The spark plug in the second cavity is not activated because no hydrogen and ethylene are injected upstream of the second cavity. Because the measuring points on the upper and lower walls are symmetrically arranged, the following pressure data is the pressure measured on the upper wall. Figure 4 shows the contour of the pressure distributions as time evolves in test A1, and the time instants of the changing equivalence ratio are denoted by two black dotted lines at 12.20 and 14.30 s, as shown in Fig. 4. Φ_1^i and Φ_2^i in Fig. 4 are the initial values of Φ_1 and Φ_2, respectively; whereas Φ_1^f and Φ_2^f are the final values of Φ_1 and Φ_2, respectively. Note that t^a denotes the time instant occurring abrupt pressure change. In test A1, fuel is only injected upstream of the first cavity, and $\Phi_2 = 0.00$ remains unchanged. At the early stage from 11.50 to 12.20 s with $\Phi_1 = 0.38$, the high pressure generated by combustion propagates to $x = 240$ mm in the isolator, in which the pressure in the first cavity and its upstream area is the highest overall and significantly higher than the pressure around the second cavity. Then, in the middle stage from 12.20 to 13.75 s, as Φ_1 linearly decreases, the combustion intensity is gradually weakened, with the high-pressure region upstream of the cavity gradually contracting to encompass the first cavity. However, at $t^a = 13.77$ s and $\Phi_1^a = \Phi_t^a = 0.14$, it shows abrupt changes of the overall pressure in the combustor. In the meantime, the high-pressure region upstream of
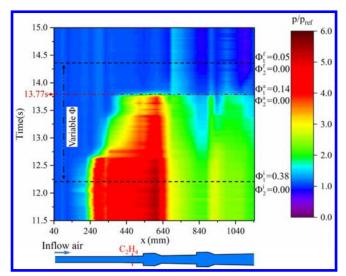
Table 2 Experimental parameters for all test cases

Test case	Φ_1	Φ_2	Φ_t
A1	0.38–0.05	0.00	0.38–0.05
A2	0.08–0.38	0.00	0.08–0.38
A3	0.28–0.07	0.09–0.09	0.37–0.16
A4	0.09–0.28	0.09–0.09	0.18–0.37
A5	0.09–0.09	0.41–0.09	0.50–0.18
A6	0.09–0.09	0.09–0.37	0.18–0.46

Fig. 4 Contour of the pressure distributions in test A1.

the first cavity disappears and the pressure in the second cavity abruptly declines. During the process of the abrupt change of pressure, the location of the maximum pressure is moved from the trailing edge of the first cavity toward the middle between the first and second cavities, indicating that the flowfield structure in the cavity changes significantly. After the abrupt change of pressure, the pressure between the multicavity continues to gradually decrease with the decrease in the equivalence ratio.

To better understand the flame variation in the combustor during the abrupt change process, CH* images at approximately 13.770 s in the test are shown in Fig. 5. The legend value reflects the relative flame strength after pseudocolor processing. At 13.765 s, the leading edge of the flame is anchored upstream of the first cavity, and the flame front exhibits an irregularly curved shape, which is a typical phenomenon of the jet-wake stabilized combustion. When the equivalence ratio is the same, the stronger flame luminosity and the larger heat release range indicate the higher combustion intensity. Due to the high combustion intensity in the first cavity and no fuel injection in the second cavity, no flame occurs between these two cavities or in the second cavity. It is noted that although the high pressure reaches upstream of the injection location, the flame is located downstream of the fuel injection location, as shown in Fig. 4, demonstrating that combustion in the first cavity at this time induces a strong shock train and the position of the head shock wave was located upstream of the heat release region. Due to the supercharging effect of the shock train, although no combustion occurs in the region between the two cavities or in the second cavity, an apparent increase in pressure still occurs. As time evolves, the upstream flame abruptly weakens and retreats at 13.775 s, and it is instantly transformed into the shear-layer stabilized combustion with the flame zone located downstream of the leading edge of the cavity. The emergence of the cavity shear-layer stabilized combustion in the first cavity suggests that the shock train structure under the jet-wake stabilized combustion disappears, which further confirms that the abrupt change in pressure, as shown in Fig. 4, is caused by the flame stabilization mode transition. In addition, once the fast flame stabilization mode transition from the jet-wake stabilized combustion to the cavity shear-layer stabilized combustion has been completed, a flame emerges at the center of the two cavities and near the position of the second cavity, and the shock train originally observed upstream of the first cavity disappears. Due to the accompanying pressure drop and flow velocity increase, the combustion intensity of the first cavity is notably reduced [35]. Therefore, the unburned fuel in the first cavity continues to burn between the two cavities, which partially compensates for the abrupt reduction in heat released due to flame stabilization mode transition in the first cavity, also explain that the pressure reduction amplitude between the two
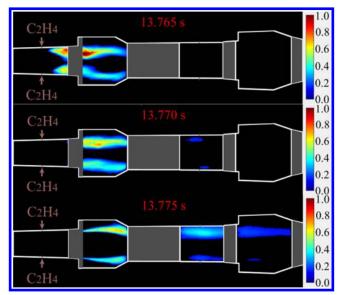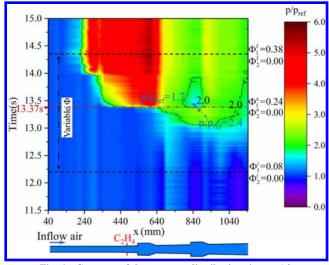

Fig. 6   Contours of the pressure distributions in test A2.

cavities is large, but the pressure reduction amplitude between the two cavities is small.

Figure 6 shows the contour of the pressure distributions in test A2 with an increased equivalence ratio when compared to that of test A1. To better understand the variation process of the pressure, an auxiliary contour line for $p/p_{\text{ref}} = 2.0$ is added to the figure. In the early stage from 12.20 to 13.37 s, the pressure in the first cavity changes slightly with increasing Φ_1, but the pressure in the second cavity gradually increases. Then, a similar abrupt change in pressure is observed in the first cavity at $t^a = 13.37$ s and $\Phi_1^a = \Phi_t^a = 0.24$. In Fig. 6, $p/p_{\text{ref}} = 1.7$ and $p/p_{\text{ref}} = 2.4$ refer to the relative pressures of two adjacent points at the boundary of the enclosed region formed by the $p/p_{\text{ref}} = 2.0$ contour line, which means the pressure near the second cavity decreases from 2.4 to 1.7 instead of suddenly increasing, as observed in test A1. Subsequently, the pressure in the first and second cavities continues to increase synchronously with increasing Φ_1. Similarly, Fig. 7 shows the CH* images at the abrupt change stage in which the flame stabilization mode transitions from cavity shear-layer stabilized combustion to jet-wake stabilized combustion from 13.360s to 13.380 s. Before the flame stabilization mode transition, the first cavity exhibits the typical flame stabilization mode of the cavity shear-layer stabilized combustion, and an obvious burning zone is observed between the two cavities and in the second cavity. Then, the combustion intensity in the first cavity
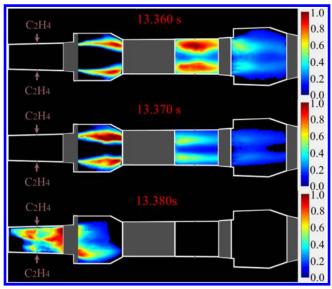

Fig. 5   Flame change occurring an abrupt change in pressure in the first cavity in test A1.

Fig. 7   Flame change occurring as an abrupt change in pressure in the first cavity in test A2.

abruptly increases, whereas the combustion intensity near the second cavity suddenly decreases and eventually reaches zero. This phenomenon occurs because the flame stabilization mode transition leads to an increase of the fuel combustion intensity and fuel burnout in the first cavity, which causes the flame out in the second cavity.

To compare the different characteristics of the abrupt pressure changes between the aforementioned two tests, Fig. 8 shows the pressure distributions before and after the flame stabilization mode transition in tests A1 and A2, where the error bars are the uncertainties of the pressure. To better standardize the pressure selection criteria, the pressure selection time before the flame stabilization mode transition is $t^a - \Delta t$, and the counterpart after the flame stabilization mode transition is $t^a + \Delta t$, where t^a is the time of abrupt pressure change in the contour and the time interval is $\Delta t = 0.04$ s. The pressure average of three representative pressure values near the selection time is used so as to eliminate the influence of pressure fluctuation. The uncertainty of the pressure measured in the experiment is calculated by the Bessel formula [36]. Moreover, p_J denotes the pressure distribution for the jet-wake stabilized combustion, and p_C is the pressure distribution for the cavity shear-layer stabilized combustion. In test A2, the pressure distributions are observed to be higher than that in test A1, regardless of the jet-wake stabilized combustion or the cavity shear-layer stabilized combustion conditions. This is due to the equivalence ratio at the time of the flame stabilization mode transition in Test A2 is $\Phi_1^a = 0.24$, which is higher than $\Phi_1^a = 0.14$ in test A1. In addition, in the flame stabilization mode transition process, the combustion intensity and pressure in test A2 with an increasing equivalence ratio are higher than the combustion intensity and pressure in test A1 with a decreasing equivalence ratio. However, due to the higher equivalence ratio for mode transition in test A2, the change range between the two stabilized combustion regimes is relatively broad. Upon the mode transition to the jet-wake stabilized combustion, the resulting pressurization of the newly formed shock train upstream is insufficient to completely compensate for the pressure loss caused by the absence of heat release. Consequently, the pressure near the second cavity decreases while an abrupt change occurs, as shown in Fig. 6, which are manifested as the pressure curves in Fig. 8 for test A2 in the region of the second cavity.

Summarizing the results of tests A1 and A2, the unburned fuel in the first cavity tends to continue to burn downstream due to the divergent flowpath with a low expansion angle. Regardless of the flame stabilization mode in the first cavity, no flame is observed in the recirculation zone of the second cavity, which suggests that the second cavity has insignificant influences on the combustion when the fuel is injected only upstream of the first cavity. Moreover,
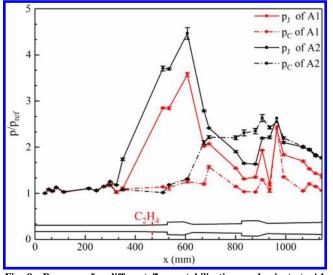
combustion and extinction happen in the vicinity of the second cavity, which does not facilitate thrust control of the combustor.

B. Influence of a Low Equivalence Ratio of Φ_2 on the Coupling Effect

To study the coupling effect of combustion in the multicavity, a constant equivalence ratio was set in the second cavity in tests A3 and A4, which is different from that of no fuel injection in the second cavity in tests A1 and A2. To prevent the flame stabilization mode in the first cavity from maintaining the jet-wake stabilized combustion due to the combustion in the second cavity, Φ_2 was set to a relatively low value of 0.09. In test A3, the initial equivalence ratios were $\Phi_1^i = 0.28$ and $\Phi_2^i = 0.09$, and the final equivalence ratio were $\Phi_1^f = 0.07$ and $\Phi_2^f = 0.09$. Figure 9 shows contour of the pressure distributions in test A3. In the early stage from 11.50 to 12.20 s, because Φ_1 remains unchanged, there are two peaks of the pressure distributions, which are consistent with the first and second cavity regions of the combustor, respectively. In the middle stage from 12.20 and 13.60 s, as Φ_1 decreases, the combustion intensity in the first cavity is weakened gradually, with the pressure in the two cavities' regions decreasing and the starting point of the high-pressure region gradually receding. At 13.61 s with $\Phi_1^a = 0.14$ and $\Phi_2^a = 0.09$, it shows an abrupt pressure drop in both the first and second cavities, in which the pressure decrement of the first cavity is notably higher than that of the second cavity. After the abrupt pressure change, the position of the high-pressure region in the combustor recedes directly from upstream of the first cavity to upstream of the second cavity, and the pressure distribution involving double peaks is transformed into a single-peak distribution. Compared to test A1, Φ_1^t remains unchanged like the flame stabilization mode transition of the first cavity in test A3, which indicates that combustion in the second cavity does not affect the combustion in the first cavity during this process.

Figure 10 shows the flame variation in the combustor during the abrupt change process in test A3. At 13.600 s, both the flame stabilization modes of the first and second cavities are the jet-wake stabilized combustion; however, they are with different formation mechanisms, in which the first cavity is owing to the substantial local heat release, and the second cavity is caused by the deceleration, pressurization, and temperature increase of the shock train upstream of the first cavity. In addition, the two combustion zones are observed to exist independently, which explains the two peaks of the pressure distribution, as shown in Fig. 9. At 13.610 s, the flame stabilization mode transition of the first cavity occurs rapidly from the jet-wake stabilized combustion to the cavity shear-layer stabilized combustion because of the decrease of Φ_1. After the flame stabilization mode transition, the flames in the first and second cavities connect due to the presence of unburned fuel, and the heat release is concentrated mainly near the second cavity. Therefore, the pressure exhibits a
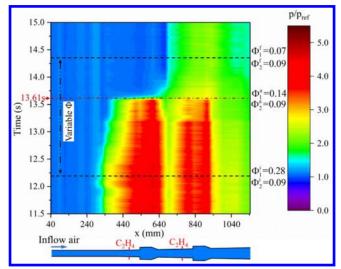

Fig. 8 Pressures for different flame stabilization modes in tests A1 and A2.

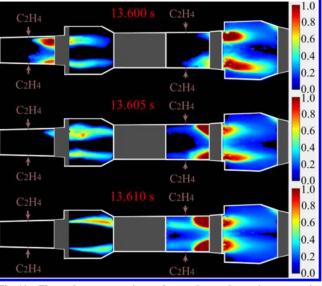**Fig. 9 Contours of the pressure distributions in test A3.**

Fig. 10   Flame change occurring under an abrupt change in pressure in the first cavity in test A3.

single-peak distribution at this time, as shown in Fig. 9. As the flame stabilization mode of the first cavity becomes the cavity shear-layer stabilized combustion at 13.610 s, unburned fuel tends to flow downstream, and a higher combustion intensity can be found in the second cavity than that at 13.600 s. This process compensates for the missing shock train pressurization effect after the flame stabilization mode transition in the first cavity. Therefore, when the pressure abruptly changes in the first cavity, the pressure in the second cavity in test A3 (Fig. 9) does not exhibit an abrupt change that is similar to the abrupt change found in test A1 (Fig. 4).

Test A4 is opposite to test A3, with Φ_1 increasing from 0.09 to 0.28 and Φ_2 being unchanged. Figure 11 shows contour of the pressure distributions in test A4. Overall, the change trend in test A4 is opposite to that of test A3 for pressure, except a difference from 12.60 to 13.43 s. The pressure propagates upstream to cross the trailing edge, the interior, and the leading edge of the first cavity in sequence; however, the propagation speed in the second cavity is slower than that observed in test A3, as shown in Fig. 9, indicating that the combustion in the second cavity affects the combustion in the first cavity through backpressure forward propagation. At a time of $t^a = 13.43$ s with $\Phi_1^a = 0.20$, $\Phi_2^a = 0.09$, and $\Phi_t^a = 0.29$, the pressure near the first cavity increases abruptly. In addition, $\Phi_1^a = 0.20$ corresponding to the flame stabilization mode transition is smaller than the corresponding value of $\Phi_1^a = 0.24$ in test A2, which also
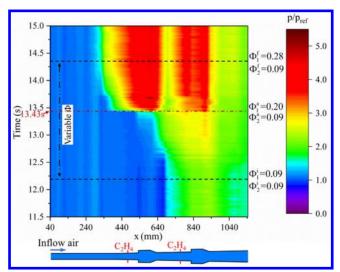
indicates that the high-pressure and low-velocity region generated by combustion in the second cavity extends to the first cavity, resulting in earlier occurrence of the flame stabilization mode transition in the first cavity.

C.   Backpressure Inducing Flame Stabilization Mode Transition

To strengthen the effect of the second cavity on the first cavity, Φ_1 is set to a constant and low value and Φ_2 varies in a wide range so as to be able to realize flame stabilization mode transition in the first cavity. Here, Φ_2 decreases in test A5 and Φ_2 increases in test A6, and $\Phi_1 = 0.09$ is fixed in two tests. The specific experimental conditions are listed in Table 2.

Figure 12 shows contours of the pressure distributions in test A5. Different from the two high-pressure regions encountered in the combustor at a high equivalence ratio in test A3, only one high-pressure region is observed in test A5. The most upstream position of the high-pressure zone has passed the fuel injection position upstream of the first cavity, which is consistent with the jet-wake stabilized combustion observed in the previous test. In addition, the highest pressure occurs near the second cavity, indicating that combustion in the second cavity is the strongest. From 12.20 to 13.10 s with decreasing Φ_2, the pressure in the first and second cavities decreases, and the high-pressure region gradually recedes toward the second cavity. At 13.15 s, with $\Phi_1^a = 0.09$, $\Phi_2^a = 0.27$, and $\Phi_t^a = 0.36$, the pressure near the first cavity abruptly decreases but the pressure near the second cavity approximately remains unchanged. For the first cavity, an apparent pressure rise influenced by the downstream combustion is observed after the flame stabilization mode transition. Then, as Φ_2 decreases, the pressure in the first and second cavities decreases, and the high-pressure region continues to retreat toward the second cavity. At 13.95 s, the range of the high-pressure region nearly remains unchanged even as Φ_2 is increasingly decreased, indicating that the pressure variation in the second cavity is insensitive to the change of Φ_2. After 14.30 s, the pressure distribution remains unchanged with a fixed equivalence ratio.

To further understand flame characteristics during the flame stabilization mode transition in the first cavity, the flame images captured in the test are analyzed, as shown in Fig. 13. According to the results of tests A1 and A2, the flame stabilization mode should be the cavity shear-layer stabilized combustion in the first cavity with $\Phi_1 = 0.09$. However, due to the influence of combustion in the second cavity, the flame stabilization mode is the jet-wake stabilized combustion in the first cavity at 13.145 s. Different from the single-peak pressure distribution in previous tests, the burning zones of the two cavities are relatively independent. It is noted that combustion in the second cavity affects the combustion and heat release characteristics of the first cavity through the backpressure forward transmission. At 13.170 s, with decreasing Φ_2, combustion in the second cavity is

Fig. 11   Contours of the pressure distributions in test A4.
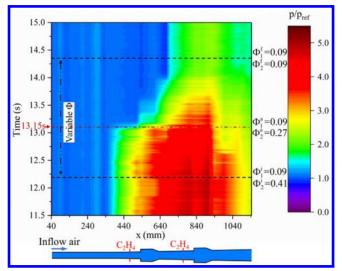

Fig. 12   Nephograms of the pressure distributions in test A5.

Fig. 13 Flame change occurring as an abrupt change in pressure in the first cavity in test A5.
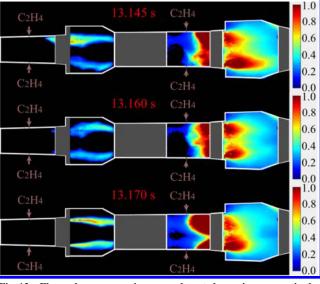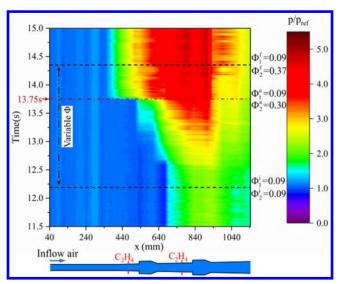

Fig. 15 Flame change occurring as an abrupt change in pressure in the first cavity in test A6.

weakened; and the generated backpressure is insufficient to sustain the jet-wake stabilized combustion in the first cavity. Therefore, the flame stabilization mode in the first cavity transitions to the cavity shear-layer stabilized combustion. Although the flame stabilization mode transition of the first cavity has been completed from the jet-wake stabilized combustion to the cavity shear-layer stabilized combustion, combustion in the second cavity remains violent, which sustains a high pressure in the second cavity. Moreover, the unburned fuel in the first cavity is further burned in the second cavity to compensate for the negative effect of the abrupt pressure drop in the first cavity on the pressure in the second cavity.

Figure 14 shows contours of the pressure distributions in test A6 with increasing Φ_2. It is similar to test A5: only one high-pressure peak was observed in test A6. With increasing Φ_2, the high-pressure region continues to extend upstream and downstream simultaneously. The pressure propagates upstream to cross the trailing edge, the interior, and the leading edge of the first cavity in sequence. At 13.75 s, for $\Phi_1^a = 0.09$, $\Phi_2^a = 0.30$, and $\Phi_t^a = 0.39$, the pressure in the first cavity abruptly increases, indicating that the combustion intensity in the first cavity is abruptly enhanced. Figure 15 shows the flame variation during the flame stabilization mode transition in the first cavity in test A6. At 13.740 s, the cavity shear-layer stabilized combustion is observed in the first cavity before the abrupt change. Then, at 13.750 s, the flame stabilization mode of the first cavity

transitions into the jet-wake flame stabilized under the influence of backpressure in the second cavity. However, this transition does not result in a significant change in the combustion intensity in the second cavity.

The results in tests A5 and A6 indicate that combustion in the second cavity affects the flame stabilization mode of the first cavity through backpressure forward transmission; however, the connection between the two burning zones is weak. The effect of the downstream pressure accounts for the flame stabilization mode transition in the first cavity. Throughout the entire flame stabilization mode transition process, the burning zones of the combustor do not change significantly. Moreover, heat release is always concentrated in the second cavity region, and the pressure distribution exhibits single-peak characteristics throughout the entire process, which are beneficial for smooth thrust transition in the combustor.

D. Analysis of the Drive Mode During Flame Stabilization Mode Transition

Based on the aforementioned results, two driving modes can be identified during flame stabilization mode transition in the first cavity: namely, direct adjustment of the local heat release for tests A1, A2, and A3; and variation of the downstream backpressure for tests A5 and A6. Furthermore, the transition process is driven by both the local heat release and downstream backpressure in test A4. The specific characteristics of the flame stabilization mode transition for all tests are listed in Table 3.

Fig. 14 Contours of the pressure distributions in test A6.

Table 3 Equivalence ratio and transition path of the flame stabilization mode transition time

Test	Flame stabilization mode transition[a,b]	Φ_1^a	Φ_2^a	Φ_t^a	$\Delta\Phi$	Driving methods
A1	J→C	0.14	0.00	0.14	0.10	Local heat release
A2	C→J	0.24	0.00	0.24		Local heat release
A3	J→C	0.14	0.09	0.23	0.06	Local heat release
A4	C→J	0.20	0.09	0.29		Local heat release and downstream back pressure
A5	J→C	0.09	0.27	0.36	0.03	Downstream back pressure
A6	C→J	0.09	0.30	0.39		Downstream back pressure

[a]J→C: Transition from jet-wake stabilized combustion into cavity shear-layer stabilized combustion.

[b]C→J: Transition from cavity shear-layer stabilized combustion into jet-wake stabilized combustion.

The flame stabilization mode transitions from the jet-wake stabilized combustion to the cavity shear-layer stabilized combustion in tests A1 and A3 are driven by the variation of the local heat release. Therefore, the equivalence ratios at the time instants of the flame stabilization mode transition have the same value of $\Phi_1^a = 0.14$. In test A2, owing to the reversed transition path of the flame stabilization mode from the cavity shear-layer stabilized combustion with a lower initial combustion intensity to the jet-wake stabilized combustion, the corresponding value of Φ_1^a reaches 0.24. Thus, different transition paths of the flame stabilization mode lead to a difference in the equivalence ratio of $\Delta\Phi = 0.10$. For tests A5 and A6, although the equivalence ratios for the flame stabilization mode transition are higher than that in tests A1 and A2, respectively, the transient equivalence ratio deviation caused by different flame stabilization mode transition paths has been reduced to $\Delta\Phi = 0.03$ owing to the cavity shear-layer stabilized combustion with a lower initial combustion intensity into the jet-wake stabilized combustion of the downstream pressure. Similarly, the transient equivalence ratio of Φ_1^a for the flame stabilization mode transition is also lower than the transient equivalence ratio of Φ_1^a in test A2, which is driven purely by local heat release. The transient equivalence ratio deviation caused by the different flame stabilization mode transition paths has been reduced to $\Delta\Phi = 0.06$ between tests A4 and A3, which is a transition situation between the local heat release-driven cases and the downstream backpressure-driven cases. In summary, compared to the method of local release variation, the method of downstream pressure variation can reduce the path dependence of the flame stabilization mode transition.

To better analyze the influence of the different fuel injection strategies on the abrupt change amplitude during the flame stabilization mode transition, an abrupt pressure difference parameter of $\Delta p = p_J - p_C$ is defined to characterize the pressure change before and after the flame stabilization mode transition. Because the pressure difference is an indirect measurement variable, the uncertainty is evaluated by the indirect measurement uncertainty formula. Figure 16 shows the distributions of abrupt pressure differences in all tests. The abrupt pressure differences in the first cavity in all tests are substantially larger than the abrupt pressure differences in the second cavity due to the flame stabilization mode transition in the first cavity. Considering that the abrupt pressure difference in the first cavity significantly influences the nonlinear change in thrust, it motivates us to do the following analysis. First, the distributions of the abrupt pressure differences corresponding to the transition from the cavity shear-layer stabilized combustion to the jet-wake stabilized combustion are higher than the counterparts corresponding to the opposite transition direction, which is induced by the difference in Φ_t^a having a higher value in tests A2, A4, and A6 than that in tests A1, A3, and A5.
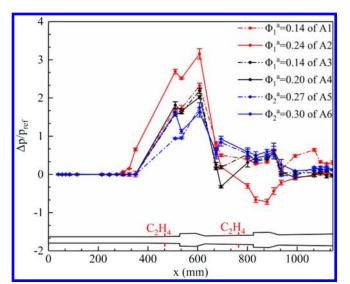
Then, by comparing tests A1, A3, and A5 with the same flame stabilization mode transition path, it reveals that the distributions of the abrupt pressure differences between tests A1 and A3 are nearly the same. Due to the same transitional equivalence ratio of Φ_1^a, the flame stabilization mode transition process is very similar. Although the total equivalence ratio in test A5 is relatively high, the abrupt pressure difference in the first cavity is smaller than that in tests A1 and A3. The pressure difference in the first cavity is the smallest among the three tests. Due to the influence of backpressure from the second cavity, the transitional equivalence ratio of Φ_1^a in test A6 is lower than that in tests A2 and A4. Therefore, the abrupt pressure difference in the first cavity in test A6 is the smallest.

To evaluate the flow and combustion characteristics in the experiment, a one-dimensional calculation method [37] was used to calculate the total pressure recovery coefficient at the outlet of the combustor to evaluate the total pressure loss under different flame stabilization modes. Table 4 shows the total pressure recovery coefficient and difference for all tests. Note that σ is the total pressure recovery coefficient and $\Delta\sigma$ is the difference of the total pressure recovery coefficient before and after the flame stabilization mode transition. First, when fuel is injected into the first cavity only, the total pressure recovery coefficient is higher but the difference between the total pressure recovery coefficient before and after the flame stabilization mode transition is also larger, corresponding to the pressure change amplitude. The difference in the total pressure recovery coefficients of experiments A5 and A6 is smaller, which is also consistent with the small change in combustion intensity in the combustor. This also proves that the flame stabilization mode transition method with the smallest change in heat release under the push of backpressure is the most suitable adjustment for the smooth change of thrust.

Based on the results, although the flame stabilization mode transition is accomplished by directly adjusting the local heat release, it is necessary to add fuel at a higher equivalence ratio locally to overcome the low combustion intensity of the cavity shear-layer stabilized combustion and accomplish the transition into the jet-wake stabilized combustion with a higher combustion intensity. The abrupt change in pressure before and after flame stabilization mode transition is directly related to the local equivalence ratio, and a high equivalence ratio will inevitably yield a large abrupt change in the pressure distribution. Therefore, the local fuel equivalence ratio can be set to a relatively low value, and the backpressure generated by downstream combustion can be employed to promote flame stabilization mode transition, which can greatly reduce the degree of abrupt pressure change. In particular, the control method of downstream backpressure instead of the direct control method of local heat release adjustment can be adopted to realize the flame stabilization mode transition and reduce the accompanied path-dependent and abrupt degree of change.

Fig. 16 Differences in pressure before and after flame stabilization mode transition in all tests.

Table 4 Total pressure recovery coefficient and difference

Test	Flame stabilization mode[a]	Φ_1^a	Φ_2^a	σ, %	$\sigma\Delta$, %
A1	J	0.14	0	22.7	4.2
	C			26.9	
A2	C	0.24	0	17.8	2.4
	J			20.2	
A3	J	0.14	0.09	19.1	−1.3
	C			17.8	
A4	C	0.20	0.09	17.2	1.2
	J			18.4	
A5	J	0.09	0.27	16.9	−0.4
	C			16.5	
A6	C	0.09	0.30	16.6	0.5
	J			17.1	

[a]J denotes jet-wake stabilized combustion, and C denotes cavity shear-layer stabilized combustion.

IV.   Conclusions

The flame stabilization mode transition influenced by different injection strategies in a combustor with a multicavity was experimentally studied based on a direct-connect supersonic combustion facility with an entrance Mach number of 3.0. Three typical injection strategies were designed for each, including two comparative experiments with increasing or decreasing equivalence ratios in an opposite manner. The variation in the pressure distributions and the dynamic flame characteristics in the combustor were measured via wall pressure and CH* luminescence imaging technology. Generally, when the flame stabilization mode transitions in the first cavity, abrupt pressure changes and path-dependent critical equivalence ratio changes are observed in all tests.

Specifically, for the first situation with fuel injection only in the first cavity, the flame stabilization mode transition of the first cavity is unaffected by combustion in the second cavity, in which different paths between the cavity shear-layer stabilization combustion mode and the jet-wake stabilized combustion mode transition cause a deviation of the critical equivalence ratios of about $\Delta\Phi = 0.10$ when the flame stabilization mode transition occurs. For the second situation with a low equivalence ratio in the second cavity, the flame stabilization mode in the first cavity transitions from the cavity shear-layer stabilization combustion to the jet-wake stabilized combustion mode. The transition time, however, occurs earlier owing to the backpressure forward transmission caused by the enhanced combustion in the second cavity. For the third situation with further strengthened combustion in the second cavity, the aforementioned deviation of the critical equivalence ratios can be reduced to $\Delta\Phi = 0.03$, which is similar to the second situation of $\Delta\Phi = 0.06$.

The driving modes of the flame stabilization mode transition of the combustor with a multicavity can be divided into two types: the direct driven by local heat release, and the indirect driven by downstream backpressure. Direct adjustment of the local equivalence ratio will lead to a large change in the burning zone of the combustor, resulting in notable path-dependent characteristics of the flame stabilization mode due to the difference in combustion intensities between the two flame stabilization modes. However, if the local fuel equivalence ratio can be set to a relatively low value, the backpressure generated by downstream combustion can be employed to realize the flame stabilization mode transition, and the change range of the burning zone can be significantly reduced. As a result, the path-dependent characteristics and abrupt degree of change induced by the flame stabilization mode transition can be greatly weakened.

Acknowledgments

References

[1] Huang, W., "Investigation on the Effect of Strut Configurations and Locations on the Combustion Performance of a Typical Scramjet Combustor," *Journal of Mechanical Science and Technology*, Vol. 29, No. 12, 2015, pp. 5485–5496.
https://doi.org/10.1007/s12206-015-1150-6

[2] Zhang, J. L., Chang, J. T., Kong, C., Qiu, H. C., and Bao, W., "Flame Oscillation Characteristics in a Kerosene Fueled Dual Mode Combustor Equipped with Thin Strut Flameholder," *Acta Astronautica*, Vol. 116, No. 8, 2019, pp. 222–233.
https://doi.org/10.1016/j.actaastro.2019.05.037

[3] Huang, W., Li, S., Yan, L., and Wang, Z., "Performance Evaluation and Parametric Analysis on Cantilevered Ramp Injector in Supersonic Flows," *Acta Astronautica*, Vol. 84, No. 11, 2013, pp. 141–152.
https://doi.org/10.1016/j.actaastro.2012.11.011

[4] Ben-Yakar, A., and Hanson, R. K., "Cavity Flame-Holders for Ignition and Flame Stabilization in Scramjets: An Overview," *Journal of Propulsion and Power*, Vol. 17, No. 4, 2001, pp. 869–877.
https://doi.org/10.2514/2.5818

[5] Wang, Z., Wang, H., and Sun, M., "Review of Cavity-Stabilized Combustion for Scramjet Applications," *Proceedings of the Institution of Mechanical Engineers, Part G: Journal of Aerospace Engineering*, Vol. 228, No. 14, 2014, pp. 2718–2735.
https://doi.org/10.1177/0954410014521172

[6] Yu, K., and Schadow, K., "Cavity-Actuated Supersonic Mixing and Combustion Control," *Combustion and Flame*, Vol. 99, No. 8, 1994, pp. 295–301.
https://doi.org/10.1016/0010-2180(94)90134-1

[7] Sun, M., Cui, X., Wang, H., and Bychkov, V., "Flame Flashback in a Supersonic Combustor Fueled by Ethylene with Cavity Flameholder," *Journal of Propulsion and Power*, Vol. 31, No. 3, 2015, pp. 976–980.
https://doi.org/10.2514/1.b35580

[8] Kanda, T., Chinzei, N., Kudo, K., and Murakami, A., "Dual-Mode Operations in a Scramjet Combustor," *Journal of Propulsion and Power*, Vol. 20, No. 4, 2004, pp. 760–763.
https://doi.org/10.2514/1.3683

[9] Donohue, J., "Dual-Mode Scramjet Flameholding Operability Measurements," *Journal of Propulsion and Power*, Vol. 30, No. 3, 2014, pp. 592–603.
https://doi.org/10.2514/1.B35016

[10] Potturi, A., and Edwards, J., "Large-Eddy/Reynolds-Averaged Navier–Stokes Simulation of Cavity-Stabilized Ethylene Combustion," *Combustion and Flame*, Vol. 162, No. 4, 2015, pp. 1176–1192.
https://doi.org/10.1016/j.combustflame.2011.10.009

[11] Huang, W., Du, Z., Yan, L., and Moradi, R., "Flame Propagation and Stabilization in Dual-Mode Scramjet Combustors: A Survey," *Progress in Aerospace Sciences*, Vol. 101, No. 6, 2018, pp. 13–30.
https://doi.org/10.1016/j.paerosci.2018.06.003

[12] Micka, D. J., and Driscoll, J. F., "Combustion Characteristics of a Dual-Mode Scramjet Combustor with Cavity Flameholder," *Proceeding of the Combustion Institute*, Vol. 32, No. 2, 2009, pp. 2397–2404.
https://doi.org/10.1016/j.proci.2008.06.192

[13] Micka, D. J., "Combustion Stabilization, Structure, and Spreading in a Laboratory Dual-Mode Scramjet Combustor," Ph.D. Dissertation, Dept. of Aerospace Engineering, Univ. of Michigan, Ann Arbor, MI, 2010.

[14] Sun, M., Wu, H., Fan, Z., Wang, H., Bai, X., Wang, Z., Liang, J., and Liu, W., "Flame Stabilization in a Supersonic Combustor with Hydrogen Injection Upstream of Cavity Flame Holders: Experiments and Simulations," *Proceedings of the Institution of Mechanical Engineers, Part G: Journal of Aerospace Engineering*, Vol. 225, No. 12, 2011, pp. 1351–1365.
https://doi.org/10.1177/0954410011401498

[15] Yuan, Y. M., Zhang, T. C., Yao, W., Fan, X. J., and Zhang, P., "Characterization of Flame Stabilization Modes in an Ethylene-Fueled Supersonic Combustor Using Time-Resolved CH* Chemiluminescence," *Proceedings of the Combustion Institute*, Vol. 36, No. 2, 2016, pp. 2919–2925.
https://doi.org/10.1016/j.proci.2016.07.040

[16] Zhang, X., Yue, L. J., Huang, T. L., Zhang, Q. F., and Zhang, X. Y., "Numerical Investigation of Mode Transition and Hysteresis in a Cavity-Based Dual-Mode Scramjet Combustor," *Aerospace Science and Technology*, Vol. 94, No. 9, 2019, Paper 105420.
https://doi.org/10.1016/j.ast.2019.105420

[17] Zhang, X., Zhang, Q. F., Wu, Z. J., Yue, L. J., Gao, Z. B., Luo, W. H., and Chen, H., "Experimental Study of Hysteresis and Catastrophe in a Cavity-Based Scramjet Combustor," *Chinese Journal of Aeronautics*, Vol. 35, No. 10, 2021, pp. 118–133.
https://doi.org/10.1016/j.cja.2021.08.008

[18] Suneetha, L., Radive, P., and Pandey, K. M., "Numerical Investigation on Implication of Dual Cavity on Combustion Characteristics in Strut Based Scramjet Combustor," *International Journal of Hydrogen Energy*, Vol. 44, No. 60, 2019, pp. 32,080–32,094.
https://doi.org/10.1016/j.ijhydene.2019.10.064

[19] Li, X. P., Liu, W. D., Pan, Y., and Liu, S. J., "Investigation on Ignition Enhancement Mechanism in a Scramjet Combustor with Dual Cavity," *Journal of Propulsion and Power*, Vol. 32, No. 2, 2016, pp. 439–447.
https://doi.org/10.2514/1.B35880

[20] Suneetha, L., Radive, P., and Pandey, K. M., "Numerical Investigation on Implications of Four Strut Injectors on Combustion Characteristics of a Doubly-Dual Cavity-Based Scramjet Combustor," *International Journal of Hydrogen Energy*, Vol. 45, No. 8, 2020, pp. 32,128–32,144.
https://doi.org/10.1016/j.ijhydene.2020.08.238

[21] Yang, Y., Wang, Z., Sun, M., and Wang, H., "Numerical Simulation on Ignition Transients of Hydrogen Flame in a Supersonic Combustor with Dual-Cavity," *International Journal of Hydrogen Energy*, Vol. 41, No. 1, 2016, pp. 690–703.
https://doi.org/10.1016/j.ijhydene.2015.11.115

[22] Zhao, G. Y., Sun, M. B., Wang, H. B., and Hao, O. Y., "Investigation of Combustion Characteristics in a Scramjet Combustor Using a Modified Flamelet Model," *Acta Astronautica*, Vol. 148, No. 4, 2018, pp. 32–40.
https://doi.org/10.1016/j.actaastro.2018.04.005

[23] Situ, M., Wang, C., and Zhuang, F. G., "Investigation of Supersonic Combustion of Kerosene Jets with Hot Gas Piloted Energy and Dual-Cavity," *40th AIAA Aerospace Sciences Meeting and Exhibit*, AIAA Paper 2002-0804, 2002.

[24] Yu, K., Wilson, K. J., and Schadow, K. C., "Effect of Flame-Holding Cavities on Supersonic-Combustion Performance," *Journal of Propulsion and Power*, Vol. 17, No. 6, 2001, pp. 1287–1295.
https://doi.org/10.2514/2.5877

[25] Fan, Z. Q., Liu, W., Sun, M. B., and Pan, Y., "Quantitative Analysis of Mixing and Combustion in the Scramjet Multi-Cavity Combustor," *Journal of Propulsion Technology*, Vol. 33, No. 2, 2012, pp. 185–192.
https://doi.org/10.13675/j.cnki.tjjs.2012.02.005

[26] Voland, R. T., Auslender, A. H., Smart, M. K., Roudakov, A. S., Semenov, V. L., and Kopchenov, V., "CIAM/NASA Mach 6.5 Scramjet Flight and Ground Test," *9th International Space Planes and Hypersonic Systems and Technologies Conference*, AIAA Paper 1999-4848, Nov. 1999.
https://doi.org/10.2514/6.1999-4848

[27] Vinagradov, V., Kobigsky, S. A., and Petrov, M. D., "Experimental Investigation of Kerosene Fuel Combustion in Supersonic Flow," *Journal of Propulsion and Power*, Vol. 11, No. 1, 1995, pp. 130–134.
https://doi.org/10.2514/3.23850

[28] Wang, L., Qian, Z. S., and Gao, L. J., "Numerical Study of the Combustion Field in Dual-Cavity Scramjet Combustor," *Procedia Engineering*, Vol. 99, No. 2. 2015, pp. 313–319.
https://doi.org/10.1016/j.proeng.2014.12.540

[29] Ben-Yakar, A., and Hanson, R., "Cavity Flame-Holders for Ignition and Flame Stabilization in Scramjet: An Overview," *Journal of Propulsion and Power*, Vol. 17, No. 4, 2001, pp. 869–877.
https://doi.org/10.2514/2.5818

[30] Cai, Z., Zhu, J., Sun, M., and Wang, Z., "Spark-Enhanced Ignition and Flame Stabilization in an Ethylene-Fueled Scramjet Combustor with a Rear-Wall-Expansion Geometry," *Experimental Thermal and Fluid Science*, Vol. 92, April 2018, pp. 306–313.
https://doi.org/10.1016/j.expthermflusci.2017.12.007

[31] Zhang, T. C., Wang, J., Fan, X. J., and Zhang, P., "Combustion of Vaporized Kerosene in Supersonic Model Combustors with Dislocated Dual Cavities," *Journal of Propulsion and Power*, Vol. 30, No. 5, 2014, pp. 1152–1160.
https://doi.org/10.2514/1.B35096

[32] Yuan, Y. M., Zhang, T. C., Yao, W., and Fan, X. J., "Study on Flame Stabilization in a Dual-Mode Combustor Using Optical Measurements," *Journal of Propulsion and Power*, Vol. 31, No. 6, 2015, pp. 1524–1531.
https://doi.org/10.2514/1.B35689

[33] Nakaya, S., Kinoshita, R., Lee, J., Ishikawa, H., and Tsue, M., "Analysis of Supersonic Combustion Characteristics of Ethylene/Methane Fuel Mixture on High-Speed Measurements of CH* Chemiluminescence," *Proceedings of the Combustion Institute*, Vol. 37, No. 3, 2019, pp. 3749–3756.
https://doi.org/10.1016/j.proci.2018.09.011

[34] Lin, K., Ryan, M., Carter, C., Gruber, M., and Raffoul, C., "Raman Scattering Measurements of Gaseous Ethylene Jets in a Mach 2 Supersonic Crossflow," *Journal of Propulsion and Power*, Vol. 26, No 3, 2010, pp. 503–513.
https://doi.org/10.2514/1.43757

[35] Cao, D. G., Brod, H. E., Yokev, N., and Michaels, D., "Flame Stabilization and Local Combustion Modes in a Cavity-Based Scramjet Using Different Fuel Injection Schemes," *Combustion and Flame*, Vol. 233, No. 11, 2021, Paper 111562.
https://doi.org/10.1016/j.combustflame.2021.111562

[36] Li, H., Ma, S., Chen, Y. M., Zou, Z. P., and Liu, H. X., "Experimental Study on Compact Heat Exchanger for Hypersonic Aero-Engine," *International Space Planes and Hypersonic Systems and Technologies Conferences*, AIAA Paper 2017-2333, 2017.
https://doi.org/10.2514/6.2017-2333

[37] Fotia, M. L., and Driscoll, J. F., "Ram-Scram Transition and Flame/Shock-Train Interactions in a Model Scramjet Experiment," *Journal of Propulsion and Power*, Vol. 29, No. 4, 2013, pp. 261–273.
https://doi.org/10.2514/1.b34486

R. D. Bowersox
Associate Editor